This is a repository copy of *Conversion of glucose to fructose over Sn and Ga-doped zeolite Y in methanol and water media*.

White Rose Research Online URL for this paper:
https://eprints.whiterose.ac.uk/187881/

Version: Published Version

Article:

Conversion of glucose to fructose over Sn and Ga-doped zeolite Y in methanol and water media

Mohamed M.M. Kashbor [a], Dedi Sutarma [a], James Railton [a], Naoko Sano [b], Peter J. Cumpson [b,c], Diego Gianolio [d], Giannantonio Cibin [d], Luke Forster [e], Carmine D'Agostino [e], Xi Liu [f,g,*], Liwei Chen [f], Volkan Degirmenci [h], Marco Conte [a,**]

[a] *Department of Chemistry, University of Sheffield, Sheffield S3 7HF, UK*
[b] *NEXUS, School of Mechanical & Systems Engineering, Newcastle University, Newcastle upon Tyne NE1 7RU, UK*
[c] *Mark Wainwright Analytical Centre, University of New South Wales, Kensington, Sydney, NSW 2052, Australia*
[d] *Diamond Light Source, Harwell Science and Innovation Campus, Didcot, Oxfordshire OX11 0DE, UK*
[e] *Department of Chemical Engineering and Analytical Science, The University of Manchester, Oxford Road, Manchester M13 9PL, UK*
[f] *School of Chemistry and Chemical Engineering, In-situ Center for Physical Sciences, Frontiers Science Center for Transformative Molecules, Shanghai Jiao Tong University, Shanghai 200240, PR China*
[g] *Syncat@Beijing, Synfuels China Co. Ltd., Huairou, Beijing 101407, PR China*
[h] *School of Engineering, University of Warwick, Coventry CV4 7AL, UK*

ARTICLE INFO

ABSTRACT

In this study, we use zeolite Y as a support for the synthesis of Sn and Ga doped zeolites aimed at the isomerization of glucose to fructose. Though these materials are inactive in water, they are active in methanol and we could ascertain a reaction pathway involving a hydride shift for the interconversion of glucose to fructose and mannose, and a Brønsted acid pathway with the formation of a methyl fructoside intermediate and its hydrolysis to fructose if water was added afterwards. By using characterizations comprising: chemisorption, XPS, XRD, HAADF-STEM and EXAFS; it was possible to demonstrate that a straightforward impregnation protocol for the preparation of our catalysts, led to Sn/Y mainly consisting of small SnO_2 clusters on the external surface of the zeolite, whereas Ga/Y consisting of highly dispersed Ga species mostly inside the zeolite pores; and a catalytic activity that appears to be dominated by Brønsted acid sites.

1. Introduction

The isomerization of sugars is a class of reactions which, if unlocked, could release the potential of the use of biomass for the synthesis of high value chemicals [1,2]. In fact, biomass is rich in sugar aldoses, mostly aldohexoses, including: glucose, arabinose, galactose, ribose and xylose, which can be converted to their five-membered ring ketose counterparts. This is relevant as carbohydrates represent the largest fraction (up to 60 %) of biomass-derived feedstock [3]. One of the most relevant transformations is the isomerization of glucose to fructose [4], as fructose is a precursor for the synthesis of large-scale chemicals such as 5-hydroxymethylfurfural and levulinic acid, which can be used in the polymers and biofuels sectors, respectively [5].

To date, Sn-doped zeolites [6,7] have shown great promise to catalyse the isomerisation of glucose to fructose, especially when large pore zeolites such as zeolite beta are used [8,9]. This is due to the presence of Lewis acid metal centres (Sn^{4+}) [6] and/or extra-framework SnO_x clusters located within the pores of zeolite beta which can influence the metal incorporation step [9]. Conversely, Ga has recently attracted great attention as an active metal centre for this kind of reaction [10], as it possesses a relatively high Lewis acidity [11]. This is considered by many to be an important parameter to carry out the isomerization of glucose and is thought to promote a hydride shift to the aldehydic carbon of glucose to form fructose [12,13]. Furthermore, this metal can, in principle, substitute aluminium species within the zeolite framework, and in turn, present in a highly dispersed form [14]. As a

---

result, this metal can lead to both intra- and extra-framework species when incorporated into a zeolite [15]. These factors prompted us to consider the use of commercially available zeolites, namely zeolite Y [16] which is significantly easier to prepare than zeolite beta, doped with both Sn and Ga, to carry out a systematic investigation of the reactivity of these materials and the reactive species for the specific step of the isomerization of glucose to fructose.

To this scope, we synthesized Sn, and Ga-doped zeolite Y and tested them alongside the parent non-doped zeolite Y in its acidic form to investigate the importance of Lewis acid metal centres formed by Sn and Ga, together with the presence of Brønsted centres in the zeolite in the presence of solvents like water, methanol and their combinations for the conversion of glucose to fructose. These catalysts could convert glucose to methyl fructoside, fructose and mannose (Fig. 1). Furthermore, our materials were characterised using an array of characterization tools, ranging from chemisorption to diffraction and spectroscopy, with the aim to identify structure-activity correlations useful for catalyst design.

2. Experimental section

2.1. Materials

Materials were used as received, without any additional purification, unless otherwise specified. Metal precursors: $Ga(NO_3)_3 \bullet xH_2O$ (Acros, Ga assay 25 wt %), $SnCl_4 \bullet 5 H_2O$ (Fisher, Sn assay 34 wt %); supports: Zeolite Y (Zeolyst International, CBV720 molar SiO_2:$Al_2O_3 = 30$); metal oxides: β-Ga_2O_3, (Acros, > 99.99 %) and SnO_2 (Acros, 99.9 %); sugars: glucose (D-(+)-Glucose, Alfa Aesar, anhydrous, 99 %), fructose (D-(-)-Fructose, Fisher, > 99 %), mannose (D-(+)-Mannose, Alfa Aesar, > 99 %), methyl fructoside (Methyl β-D-fructofuranoside, MuseChem, 98 %); solvents: methanol (Fisher, HPLC Grade, > 99.9 %), deionised water was obtained using a Elgastat Option 3B unit with a resistivity of 1 MΩ cm^{-1} at neutral pH.

2.2. Catalyst preparation

Gallium and tin doped zeolite Y catalysts, here denoted as Ga/Y and Sn/Y respectively, were prepared using a wet impregnation protocol with water as the solvent for the dissolution and impregnation of metal precursors into the zeolite [17]. Zeolite Y was used in its acidic form, here denoted as HY. The metal precursors used to prepare Ga/Y and Sn/Y were $Ga(NO_3)_3 \bullet xH_2O$, and $SnCl_4 \bullet 5H_2O$ respectively.

The catalysts were prepared with a final metal loading of 1 wt %, and the desired amount of metal precursor was dissolved in water (25 mL) and mixed with zeolite Y (ca. 2 g) under vigorous stirring. The amount of zeolite was adjusted to compensate for the metal assay for each precursor. The resulting slurry was heated up slowly to 80 °C and evaporated to dryness. Each catalyst was then dried at 120 °C for 16 h and calcined at 550 °C for 4 h in static air (temperature ramp 20 °C min^{-1}).

2.3. Catalytic tests

2.3.1. One-pot reaction with water or methanol as a solvent

The catalyst was dispersed in solutions containing 4 mL of water or methanol and 125 mg of glucose (α-D-glucose). The amount of catalyst, typically ca. 75 mg, was adjusted to a molar metal to glucose ratio of 1:100 with respect to the total amount of Ga or Sn in the zeolite.

Unless otherwise specified, the catalytic tests were carried out in a sealed pressure tube (Ace-type GPE Scientific) at a reaction temperature of 100 °C and reaction time of 1 h. The tube containing the reaction mixture was inserted into a pre-heated, temperature calibrated, aluminium block for the desired reaction time and equipped with a magnetic stirrer operating at 700 rpm. After the desired reaction time, the reaction mixture was quickly cooled down to room temperature by immersing the pressure tube in an ice bath.

Control tests using fructose and mannose as the reaction substrate respectively, were carried out in an identical manner to those described for glucose.

2.3.2. Two-pot reaction with methanol and water as solvents

We have observed that the use of water as a solvent does not lead to any catalytic activity (we speculate this may be due to a site-blocking effect within the pores of the zeolites). In contrast, the use of a protic organic solvent like methanol activates the zeolites, but could also lead to the formation of an alkyl fructoside intermediate. As these kinds of intermediates, if present, can be hydrolysed in water in acidic media to form fructose, this prompted us to use a two-step synthesis approach. To use methanol to start the reaction and form a reactive intermediate that can be afterwards decomposed to fructose by the addition of water. In view of this, in the first step, methanol was used as a solvent as described in the section above. After cooling the reaction mixture to room temperature using an ice bath, the vial was opened, and 4 mL of water was added into the reaction mixture. The vial was sealed and the tube reheated at 100 °C for 1 h, before being quickly cooled down to room
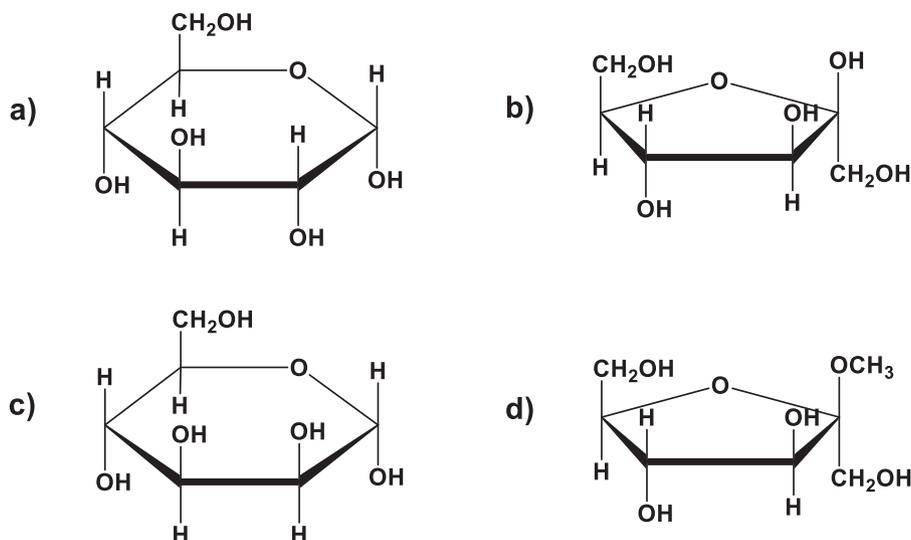
Fig. 1. (a) α-D-glucose, (b) α-D-Fructose, (c) α-D-mannose and (d) methyl β-D-fructofuranoside in their closed ring structure. α-D-glucose was the substrate used for our catalytic tests. The two furanoses glucose and mannose differ for the conformation of one stereogenic centre only (carbon in position 2), and as such they are classed as epimers.

temperature again by re-immersing the pressure tube in an ice bath, at the end of the reaction.

All catalytic tests were repeated three times to acquire the average and standard deviation of the sample of data.

2.4. Characterization of the reaction mixtures

High performance liquid chromatography was used for the characterization of the reaction mixtures, using a Shimadzu UFLC XR chromatographer. A method for a fine resolution of the reaction mixture and identification of impurities, made use of a Phenomenex Rezex RCM-Monosaccharide Ca++ column 300 by 7.8 mm, column temperature of 60 °C, and a mobile phase consisting of purified water running an isocratic elution program at a flow rate of 0.6 mL min^{-1} over 25 min and injection volume of 10 μL.

The HPLC apparatus was equipped with an evaporative light scattering detector (ELSD) [18], and the respective sugar concentrations were calculated with respect to external standards against calibration plots.

HPLC-MS for the identification of intermediates was carried out by using an Agilent 1260 Infinity liquid chromatographer, coupled with an Agilent 6530 Q-ToF mass spectrometer. The chromatographer was equipped with an Agilent Zorbax Extend-C18 column and the separation of the compounds was carried out by using a water/formic acid (0.1 %) and acetonitrile mobile phase with a gradient of acetonitrile from 5 % to 15 % in 15 min. A flow rate of 0.4 mL min^{-1} and an injection volume of 1.0 μL were used.

Conversion, observed selectivity and carbon mass balance were calculated according to Eqs. eq.s1-eq.s8.

2.5. Catalyst characterization

2.5.1. Acidity determinations

Total Brønsted acidity was determined according to [19] and references therein. 100 mg of catalyst was stirred in a sealed container with 10 mL of standardised NaOH (0.135 M) at 40 °C overnight. The solution was then recovered, and the catalyst residue was washed with 10 mL of de-ionised water which was collected by filtration. The filtrate together with the solution was back titrated with standardised HCl (0.128 M) using methyl orange as an indicator. NaOH and HCl were standardized by using potassium acid phthalate (HKC$_8$H$_4$O$_4$) and sodium carbonate (Na$_2$CO$_3$) respectively [20].

NH$_3$ chemisorption experiments were conducted using a Micromeritics ASAP 2020 instrument equipped with a Chemi 2020 Kit for the determination of NH$_3$ adsorption isotherms, based on volumetric gas sorption at different pressures, according to the protocol reported by Ding et al., [21]. Using the volume of adsorbed gas, and converting it to moles at standard temperature and pressure, allows to quantitatively measure the amount of strong Brønsted and both strong and weak Lewis acid sites in the materials. About 500 mg of the catalyst was evacuated at 150 °C for 2 h followed by adsorption measurements at 35 °C to promote the adsorption to both strong and weak sites, at gas pressures from 100 to 700 mm Hg.

In situ DRIFTS measurements were performed with a Bruker Vertex 70 FTIR spectrometer equipped with a liquid N$_2$-cooled detector. Approximately 25 mg of the catalyst sample of interest was placed in a ceramic crucible in the DRIFTS cell. Prior to the experiments, the catalyst was pre-treated by heating in Ar with a total flow rate of 50 cm^3 min^{-1} up to 400 °C for 1 h and then cooled down in flowing Ar to 35 °C. The IR spectrum of the catalyst at 35 °C under flowing Ar was taken as a background.

Gaseous pyridine in Ar was then flowed over the catalyst with a total flow rate of 50 cm^3 min^{-1} (Ar flow = 30 cm^3 min^{-1}, pyridine flow = 20 cm^3 min^{-1}) for 60 min. The temperature of the DRIFTS cell was then increased in increments of up to 150 °C. The use of pyridine was preferred to the use of ammonia as the latter can decompose over Al

centres in the presence of residual oxygen [22].

In situ DRIFTS spectra were recorded with a resolution of 4 cm^{-1} and with the accumulation of 128 scans every 60 s during transient switches. The DRIFTS spectra were analysed using the OPUS software.

2.5.2. Porosimetry and BET surface area

The pore size was determined using a Micromeritics 3Flex gas sorption system operating with liquid nitrogen at 77 K. The samples (*ca.* 100 mg) were degassed at 180 °C for 48 h before analysis. The BET surface area was calculated from the adsorption isotherm using a 20-points method and 0.162 nm^2 as the surface area for gaseous molecular nitrogen [23].

2.5.3. XRPD

X-ray powder diffraction (XRPD) patterns were acquired using a Bruker D8 Advance diffractometer equipped with a LynxEye detector. The samples were deposited over an amorphous silicon sample holder. The instrument was operating at 40 kV and 40 mA selecting the CuK$_\alpha$ radiation (1.5406 Å) as X-ray source. The samples were analysed in the 2θ range 5–80° for a scan time of 70 min. Analysis of the patterns was carried out using X-Pert Pro software.

The goodness of fit between experimental and simulated XRPD patterns was evaluated *via* χ^2-test [24] using Rietveld refinement [25] as a full-pattern fit algorithm. Initial atomic coordinate values to perform the fit were obtained using crystallographic information files (CIF) available at the Data-base of Zeolite Structures (IZA-SC) [26].

2.5.4. XPS

X-ray photoelectron spectroscopy (XPS) was performed with a Kratos Axis Nova spectrometer using a monochromatised AlK$_\alpha$ X-ray source (225 W) with an analyser pass energy of 160 eV for survey scans and 20 eV for high resolution scans. Three positions per sample were analysed using charge neutralization. All XPS spectra were charge corrected by setting the C1s C-C/H component to 284.8 eV [27].

2.5.5. ICP-MS

Determination of Sn and Ga content was carried out *via* inductively coupled plasma and mass spectrometry (ICP-MS) analysis using an Agilent 7500CE ICP-MS instrument which was calibrated up to 10 parts per billion (ppb) with solutions prepared by dilution from stock solutions containing 1,000 parts per million (ppm) of Ga or Sn standards. The concentrations of Ga and Sn in the samples were calculated against a calibration graph. Experimental values for the dopant metal content were determined at 1.0 wt % and 0.9 wt % for Sn and Ga respectively, against an expected loading of 1 wt % for each of them.

2.5.6. HAADF-STEM

Samples were prepared for transmission electron microscopy (TEM) analysis by dispersing and sonicating the catalyst powders in high purity ethanol for *ca.* 10 min, and allowing a drop of the suspension to dry on a Cu grid. HAADF-STEM images were acquired using a FEI Talos F200X operating at 200 keV under STEM mode. The frequency count for the particle size distribution for Sn/Y was obtained from a set of 200 particles. Statistical analysis was not possible for Ga/Y due to the high dispersion of Ga species. Data analysis and fitting of the particle size distributions was carried out by using OriginPro 2017 software.

2.5.7. EXAFS

Extended X-ray absorption fine structure (EXAFS) spectra were collected at the Sn K-edge (29,200 eV) and Ga K-edge (10,367 eV). Data were obtained from experiments at the beamline B18 of the Diamond Light Source, UK [28]. The measurements were carried out using a fixed-exit double-crystal Si(311) monochromator and Pt-coated branch of collimating mirrors for Sn, while Si(111) and Cr-coated branch were used for Ga. The beam size at the sample position was approximately 1 × 1 mm. All samples were prepared in forms of pellets (13 mm

diameter) using 200 mg of sample powder to maximize the edge jump (0.25 for Ga and 0.56 for Sn), maintaining the total transmission higher than 10 %. The measurement was performed at room temperature in transmission mode using 3 ion chambers filled with different gas mixtures optimized for best detection efficiency at the two edges (for Sn K-edge I_0: 50 mbar Kr/He I_t,I_{ref}: 200 mbar Kr/He, for Ga K-edge I_0: 40 mbar Ar/He I_t,I_{ref}: 200 mbar Ar/He 10 % absorption on I_0 and 70 % absorption on I_t,I_{ref}). The spectra were collected in quick EXAFS mode by continuously scanning the monochromator with a constant energy step size of 0.3 eV. The scan covered an energy range from -200 to $+1,000$ eV with respect to the edge position, corresponding to a k-range of *ca* 16 Å^{-1}. For each sample, 10 scans were acquired and subsequently merged to improve the signal to noise ratio. Data were normalized using the program Athena [28], with a linear pre-edge and 2nd order polynomial post-edge. After background subtraction the resulting $\chi(k)$ functions were k^3-weigthed and Fourier transformed in a range from 2.5 to 15.5 Å^{-1}. Fits were performed with Artemis software part of IFEFFIT suite [29]; phases and amplitudes were calculated with FEFF code [30].

3. Results and discussion

3.1. Catalytic tests using water as a solvent

Zeolite Y in its acidic form HY, and zeolite HY doped with Sn or Ga - here denoted as HY, Sn/Y and Ga/Y respectively - were systematically tested for the isomerization of glucose to fructose by using an array of conditions (see Section 3.2). When water was used as a solvent both in a single step procedure, as well as by mixing water and methanol from the beginning of the reaction, no product formation was observed under our reaction conditions (temperature range of 80 °C – 120 °C, endogenous pressure and reaction time up to 2 h). The lack of reactivity of zeolites for the isomerization reaction of glucose in water is not unprecedented [31] and it has been so far postulated to be a consequence of site blocking effects, either by strongly adsorbing inside the pores of the zeolites [32], or to Lewis Al, Sn and Ga centres or metal oxide clusters at the external surface of the zeolite [33]. We speculate the same effects take place for our materials.

3.2. Catalytic tests using methanol as a solvent

In contrast, HY, Sn/Y and Ga/Y, were highly active when methanol was used as the solvent, (Table 1), with a high catalytic activity under relatively mild reaction conditions (temperature range of 80 °C – 120 °C, endogenous pressure and reaction time of 1 h). In particular, if the reaction is carried out at 80 °C the reaction shows an equilibrium trend with conversions in the range of *ca.* 50 %, (K$_{eq}$ values for the isomerization of glucose to fructose only are in the range of 1.1 at 60 °C [34]); whereas by reaching 120 °C the reaction is nearly quantitative in the consumption of glucose. Selectivities of fructose, methyl fructoside, and mannose of *ca.* 31 %, 42 %, and 27 % were observed respectively in the case of Ga/Y at 120 °C. However, there was also a significant decrease in carbon mass balance, probably due to the formation of humins [35].

Concerning the selectivities at low temperature, the formation of methyl fructoside is largely promoted (*ca.* 70 %), whereas by reaching 120 °C this intermediate is largely decomposed (*ca.* 40–50 %) to form fructose (*ca.* 30 %), we noticed however that the higher the temperature the higher the formation of by-product mannose (up to *ca.* 20–30 %). Based on our data, a reaction temperature of 100 °C probably represents the best compromise in terms of high conversion (> 90 %) and high carbon mass balance (also > 90 %) (Table 1) or yield (Table S1).

This enhanced reactivity, however, does need to be carefully evaluated. In fact, the presence of an alcohol can well lead to an increase in conversion due to solvent effects, but it can also lead to the formation of an alkyl fructoside intermediate [36], which can, in turn, lead to two distinct reaction pathways. The first one, is the isomerization of glucose

Table 1

Catalytic tests for the isomerization of glucose to fructose in methanol, by using HY, Sn/Y and Ga/Y catalysts. The tests were carried out using 125 mg of substrate in 4 mL of CH$_3$OH at the specified reaction temperature for 1 h and endogenous pressure using a constant metal to substrate molar ratio M:S = 1:100. Experimental error reported as standard deviation of three repeated measurements.

T (°C)	Catalyst	Conversion (%)	Selectivity[a] (%)			CMB[b] (%)
			Fructose	MeF[c]	Mannose	
120	HY	94 ± 1	26 ± 1	48 ± 1	27 ± 1	76 ± 5
100	HY	90 ± 1	30 ± 2	35 ± 2	36 ± 1	99 ± 6
90	HY	70 ± 2	21 ± 2	66 ± 2	14 ± 1	95 ± 4
80	HY	49 ± 5	15 ± 6	80 ± 5	6 ± 1	97 ± 2
120	Sn/Y	96 ± 1	26 ± 1	51 ± 1	24 ± 1	67 ± 5
100	Sn/Y	95 ± 1	28 ± 1	40 ± 1	32 ± 1	84 ± 4
90	Sn/Y	71 ± 3	20 ± 1	69 ± 2	11 ± 1	93 ± 4
80	Sn/Y	50 ± 1	26 ± 1	68 ± 1	6 ± 1	100 ± 3
120	Ga/Y	98 ± 1	31 ± 1	42 ± 1	27 ± 1	50 ± 6
100	Ga/Y	94 ± 2	27 ± 2	42 ± 1	31 ± 2	91 ± 6
90	Ga/Y	62 ± 1	22 ± 3	71 ± 4	8 ± 1	92 ± 4
80	Ga/Y	55 ± 4	17 ± 2	77 ± 3	6 ± 1	98 ± 3

[a] *Observed* selectivity.
[b] CMB = (Carbon mass balance)
[c] MeF = (Methyl Fructoside)

to fructose promoted by Lewis acid centres, and the second one, either to a methyl glucoside or a methyl fructoside promoted by Brønsted acid centres (Figs. 2 and 3a and 3b).

It is worth noting that the presence of alkyl-sugar species has proven to be controversial so far. For instance, studies by Adachi, Bermejo-Deval and Davis [9,32,37] did not detect any alkyl fructoside after the reaction was carried out in methanol, with a reaction mixture comprising only: glucose, fructose and mannose were observed and reported. Other authors like Saravanamurugan [16], detected the presence of an alkyl fructoside after reaction in methanol, and this was deliberately used afterwards to obtain fructose from a hydrolysis of this intermediate.

In view of this disagreement in literature, the reaction mixture was characterised by means of HPLC-MS (Fig. S1) and a compound with molecular ion (including Na$^+$ from the ionization process) of $m/z = 217$ was identified, compatible indeed with methyl glucoside or methyl fructoside ($[C_7H_{14}O_6Na]^+ = 194 + 23 = 217$ a.m.u), with a fragmentation pattern consistent to a methyl fructoside standard (Fig. S2). It should be noted, however, that once a $[OCH_3]^+$ fragment is lost, both glucose and fructose can evolve with a similar MS fragmentation pattern [38]. As such, an additional comparison of the chromatographic retention times (Fig. S3) by means of the same standard (MuseChem) confirmed, within experimental error, the presence (quantified > 50 mol %) of methyl fructoside in our reaction mixtures.

This confirms the presence of at least two independent reaction pathways: a Lewis-catalysed glucose to fructose isomerisation, and a Brønsted-catalysed pathway to a methyl fructoside intermediate.

However, in our reaction mixtures, we also detect significant amounts (up to 25 mol %) of mannose. Mannose and glucose are epimers, that is, they are isomers that differ due to a chiral inversion in one stereogenic centre only. This epimerization reaction has been postulated to occur in two ways: (i) a carbon shift from glucose [39], (Fig. 4a), or a
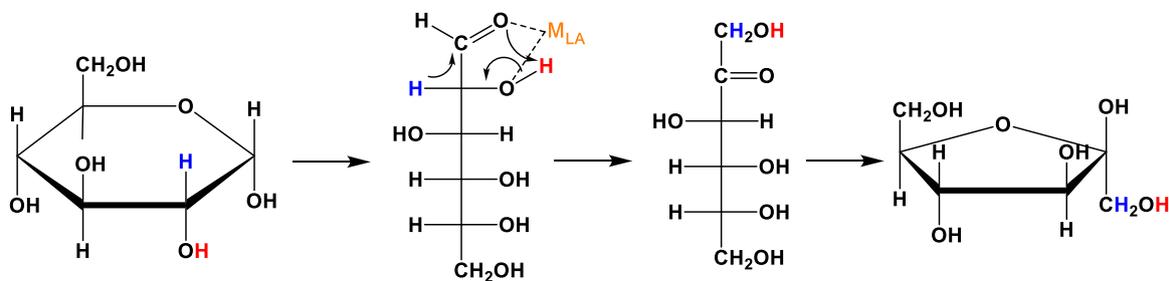
Fig. 2. Postulated Lewis acid catalysed isomerization of glucose to fructose. After ring opening a Lewis acid metal centre (M_{LA}) can coordinate the two oxygens of the carbonyl and adjacent OH group. This would induce the migration of a hydride (H atom in blue) to the aldehydic carbon, by forming a CH_2OH group and a ketone. The linear form of fructose would then close to form its ring structure.
(scheme adapted from [12]).
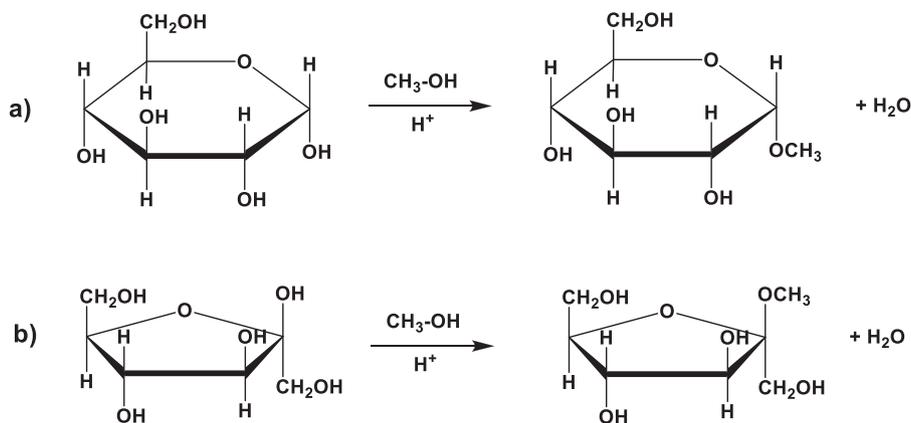
Fig. 3. Acid mediated formation of: (a) methyl glucoside and (b) methyl fructoside from the addition of CH_3-OH. Compounds in cyclic forms, originating by OCH_3 addition to the carbonyl group (aldehyde) of glucose and (b) methyl fructoside from the addition of CH_3-OH to the carbonyl group (ketone) of fructose.
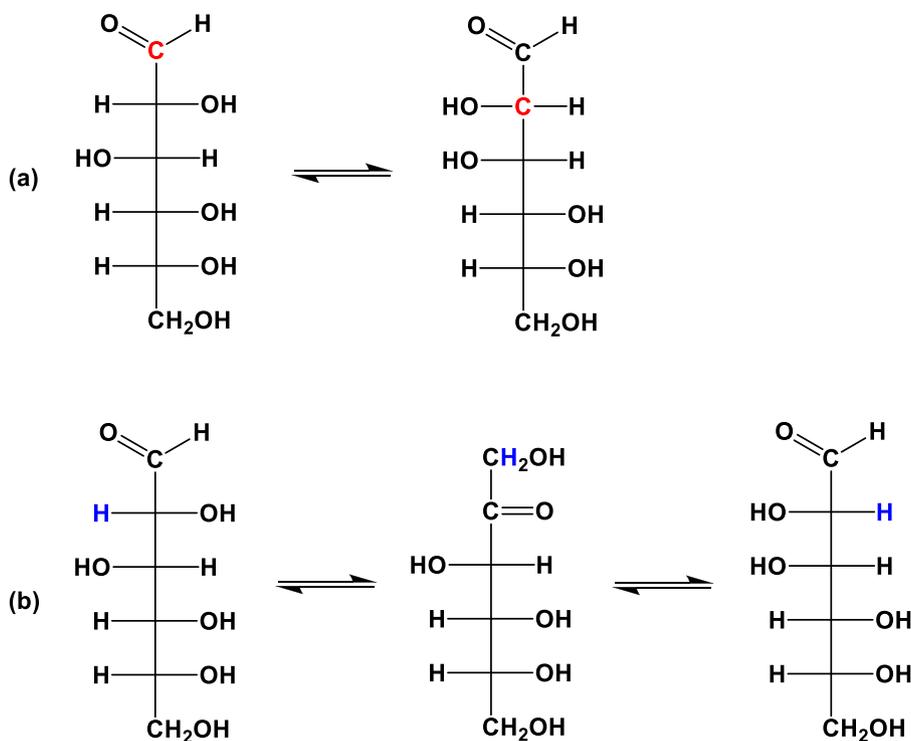
Fig. 4. (a) postulated formation of mannose from glucose *via* a carbon shift from C1 to C2; (b) postulated formation of mannose as a consequence of two sequential hydride shifts: the first from C1 to C2 from glucose to form fructose, then a further hydride shift from C2 to C1 to form mannose.

sequential hydride shift from fructose by reversing the C2 chirality [40], (Fig. 4b).

In order to elucidate which of these two mechanisms are taking place, and in turn, gather comprehensive mechanistic information about the reaction pathways that may simultaneously take place in our reaction, we carried out control tests in methanol by using fructose and mannose as substrates (Table 2).

At first, it is possible to observe that fructose entirely interconverts into methyl fructoside. This implies that in the reaction when glucose is used as a substrate, first fructose is formed (Lewis catalysed) and then this is further converted into its fructoside counterpart (Brønsted catalysed).

Then, when mannose is used as a substrate, we detect both glucose and methyl fructoside. However, from the test with fructose as a substrate, the methyl fructoside can be obtained from fructose itself. Therefore, of the two possible mechanisms for the mannose formation from glucose: (i) direct formation of mannose from glucose *via* C-shift, or (ii) the indirect conversion of glucose to mannose *via* hydride shift from fructose; the acquired data support the second mechanism, as the first one would not lead to the detection of any alkyl fructoside.

In summary, we can then schematize the isomerization reaction of glucose in methanol as the consequence of the following multiple equilibria (Eqs. 1–3):

$$\text{Glucose} \rightleftarrows \text{Fructose; Lewis-catalysed} \qquad (1)$$

$$\text{Fructose} \rightarrow \text{Methyl-Fructoside; Brønsted catalysed} \qquad (2)$$

$$\text{Glucose} \rightleftarrows \text{Fructose} \rightleftarrows \text{Mannose; Lewis catalysed} \qquad (3)$$
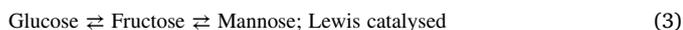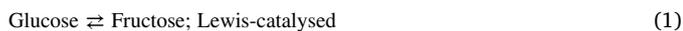
Bearing these mechanisms in mind and the product distribution that we detect, it would seem that any Lewis acid effect induced by the metal dopants Ga or Sn is negligible compared to the effect of pre-existing Al centres, and the product distribution is mainly dominated by Brønsted acidity for the formation of methyl fructoside. There seems however to be differences in by-products with Ga/Y possibly promoting the formation of humins at 120 °C as no 5-HMF was detected at the reaction conditions used.

3.3. Catalytic tests in a two-steps protocol by using methanol and water

Having confirmed the presence of methyl fructoside intermediate in the reaction mixtures as a consequence of the acid-mediated attack of methanol to fructose, a sequential hydrolysis of this compound by water to form and enhance the formation of fructose was considered (Fig. 5) [16]. It should be noted that this step is also Brønsted acid catalysed. The results of this sequential reaction are reported in detail in Table 3 and Table S2, and also in this case we verified that the reaction was at equilibrium after 1 h.

Firstly, the most evident effect of the addition of water is the consumption of methyl fructoside to form fructose. From our data, the decrease of methyl fructoside intermediate practically matches, within

experimental error, the formation of fructose, and leading to a formation of *ca.* 40–70 % of fructose for the tests carried out at 100 and 120 °C (Table 3) and fructose yields in the range of 50 % (Table S2). Secondly, for all catalysts HY, Sn/Y and Ga/Y, the conversion is not affected by this water treatment which suggests that after the first step, the reaction reached equilibrium and any changes in selectivity seen are due to the hydrolysis reaction only. To confirm this conclusion, kinetic profiles were obtained for all catalysts both in methanol and using the two-pot methanol followed by water reaction protocol considering reaction times from 0 h to 2 h (Figs. S4–S9). Both the reactions are practically concluded after approximately 40 mins, confirming that the reaction in methanol was indeed at completion after 1 h and any changes in the obtained selectivities followed by the addition of water are not due to an insufficient reaction time during the first step. Thirdly, the second step does not significantly affect the mannose selectivity (either formation or consumption) for all of the catalysts. This is noteworthy as for the reactions at 100 and 120 °C, the conversion (> 90 %) is so high as to consider the reaction as nearly quantitative. For the reactions at 80 °C and 90 °C the glucose conversion is, and remains, in the range of 60 % regardless of the presence of water. Therefore, it is reasonable to conclude that this solvent does not alter the equilibria (mainly epimerization) of any of the species involved in this reaction, but only the alkyl fructoside to fructose hydrolysis.

In view of the relevance that the methyl fructoside intermediate appears to have to the formation of fructose, further improvements towards an enhanced fructose selectivity could include an increase in the reaction temperature, and endogenous pressure, for the reaction step after the addition of water, as well as a lower pH to promote the hydrolysis of the alkyl fructoside or the use of zeolites with higher Brønsted acidity. The latter option, however, could also promote the formation of undesired humins. As a consequence, a careful determination and evaluation of possible reaction conditions for optimization purposes will be necessary and will form the basis of future work.

3.4. Control tests for leaching and mass transfer

In order to validate our results, control tests for leaching and mass transfer limitations were carried out. Although the activity of the materials studied seems to be dominated by Brønsted acidity, the possibility of leaching effects must also be considered [11]. By analysing the reaction mixtures for traces of Ga and Sn *via* ICP analysis at every reaction step, extremely small metal leaching values were observed, with a Ga mass loss < 0.1 % (relative to the total amount of Ga in the catalyst) for both the methanol and water addition step, and a relative metal mass loss of 1.2 % and 1.7 % for Sn/Y after the methanol and water addition step respectively. To rule out any effect of these small amounts of metals in solution, we tested reaction mixtures containing $SnCl_4 \cdot 5H_2O$ and $Ga(NO_3)_3 \cdot xH_2O$ precursors. Catalytic tests were carried out using the same trace amounts of metal leaching detected above (approximately corresponding to a metal to substrate molar M:S ratio of $1:10^2$ for Ga and $1:10^4$ for Sn). No catalytic activity was detected during these tests.

Catalytic tests using varying mixer stirring rates in the range 100–1,000 rpm also did not show any effect, whereas a change in M:S ratio from 1:10–1:1,000 did (Fig. S10). As such, it can be confirmed that an MS: 1:100 is appropriate for this reaction *i.e.* our catalytic tests were carried out under a kinetic regime and negligible mass transfer diffusion limitation.

3.5. Characterization of the catalysts and structure-activity correlations

In view of the multiple reaction pathways that we have identified to be possible for the formation of fructose (eqs. 1–3), either involving hydride shift or an acid/base pathway, and that some of these could occur inside or outside the pores of the zeolites, our catalytic data prompted us to study and identify possible structure-activity correlations for these catalysts. Therefore, these were systematically

Table 2

Control tests for the isomerization of sugars by using fructose and mannose as substrates in methanol. The tests were carried out using 125 mg of substrate in 4 mL of CH_3OH at a reaction temperature of 100 °C for 1 h and endogenous pressure at a constant metal to substrate molar ratio M:S = 1:100.

Catalyst	Substrate	Conversion (%)	Selectivity (%)		
			Me-fructoside	Glucose	Mannose
HY	Fructose	100	100	0	0
Sn/Y	Fructose	100	100	0	0
Ga/Y	Fructose	100	100	0	0
			Me-fructoside	Glucose	Fructose
HY	Mannose	90	82	18	0
Sn/Y	Mannose	93	84	16	0
Ga/Y	Mannose	91	85	15	0

Fig. 5. Formation of fructose from methyl fructoside by hydrolysis in water (acid catalysed).

Table 3

Catalytic tests for the isomerization of glucose to fructose in methanol followed by the addition of water in a two-step procedure using HY, Sn/Y and Ga/Y catalysts. The tests were carried out using 125 mg of substrate in 4 mL of CH_3OH at a reaction temperature for 1 h and endogenous pressure, and then adding 4 mL of H_2O for an additional reaction time of 1 h at a constant metal to substrate molar ratio M:S = 1:100. Experimental error reported as standard deviation of three repeated measurements.

T (°C)	Catalyst	Conversion (mol%)	Selectivity[a] (mol%)			CMB[b] (%)
			Fructose	MeF[c]	Mannose	
120	HY	92 ± 1	54 ± 1	18 ± 1	28 ± 1	80 ± 4
100	HY	86 ± 2	40 ± 2	26 ± 2	34 ± 1	93 ± 5
90	HY	69 ± 1	25 ± 6	61 ± 4	14 ± 1	93 ± 3
80	HY	42 ± 4	21 ± 1	66 ± 1	4 ± 1	100 ± 2
120	Sn/Y	93 ± 1	56 ± 1	20 ± 1	25 ± 1	65 ± 6
100	Sn/Y	90 ± 3	50 ± 2	25 ± 4	25 ± 1	77 ± 4
90	Sn/Y	70 ± 1	23 ± 1	67 ± 1	10 ± 1	84 ± 4
80	Sn/Y	47 ± 3	26 ± 5	72 ± 5	3 ± 1	97 ± 2
120	Ga/Y	96 ± 1	67 ± 1	14 ± 1	21 ± 2	63 ± 4
100	Ga/Y	91 ± 4	55 ± 1	20 ± 2	25 ± 2	93 ± 5
90	Ga/Y	56 ± 2	26 ± 4	68 ± 4	7 ± 1	94 ± 3
80	Ga/Y	54 ± 6	20 ± 1	77 ± 1	2 ± 1	87 ± 5

[a] *Observed* selectivity
[b] CMB = (Carbon Mass Balance)
[c] MeF = (Methyl Fructoside)

investigated, by using an array of acidity measurements and techniques like XPS, ICP-MS, XRPD, HAADF-STEM and EXAFS.

3.5.1. Acidity measurements

Due to the relevance of acidity in the data collected so far, the materials were characterised for both Brønsted and Lewis acidity. The total Brønsted acidity was determined using a back-titration protocol (see experimental Section 2.5.1.); whereas the combination of Brønsted and Lewis acidity was determined using an NH_3 chemisorption protocol

Table 4

Acidity and textural properties of HY, Sn/Y and Ga/Y: (a) total Brønsted acidity determined by back-titrations; (b) total Brønsted and Lewis acidity by NH_3 chemisorption; (c) Lewis to Brønsted acid sites ratio from DRIFT measurements (d) surface area by a 20 points BET method using N_2 adsorption and (e) microporous volume determined by BJH method using N_2 adsorption.

Catalyst	B acidity [a] (mmol g^{-1})	B + L acidity [b] (mmol g^{-1})	L/B ratio [c]	S [d] (m^2 g^{-1})	V$_{micro}$ [e] (mL g^{-1})
HY	1.78	2.93	0.95	797	0.26
Sn/Y	1.72	2.85	0.89	691	0.21
Ga/Y	1.70	2.78	1.2	695	0.21

(Table 4, and Fig. S11). The use of a back-titration for the determination of the acidity of solids, although simple is a straightforward and statistically robust method, which still finds application for the determination of the titratable acidity of microporous polymers [41,42]. That is: for the determination of the number of protons recovered during titration with a strong base to a specified endpoint [43], which in our case corresponds to Brønstead acidity.

Brønsted acidity can originate from OH groups by SiOH units or hydrated Al centres [44], whereas Lewis acidity can originate from coordinatively unsaturated Al, Sn or Ga centres [45]. From our data, there is an apparent decrease in Brønsted acidity upon metal doping. In theory, this is consistent with a decrease in Brønsted acidity due to the formation of basic SnO_2 and Ga_2O_3. However, the difference among these values (1.78–1.70 mmol g^{-1}) is within the experimental error of our method (*ca.* 0.02 mmol g^{-1}), and as such this difference is not considered to be statistically different.

With respect to the combination of Brønsted and Lewis acidity instead, measured by NH_3 chemisorption, there is also a decrease in the total acidity. A comparison between Brønsted acidity from back-titration and total Brønsted and Lewis acidity from chemisorption is not straightforward, although our data would suggest there is no obvious difference in Lewis acidity among our materials. The two sets of data from back-titration and NH_3-chemisorption are consistent with each other though, as NH_3 chemisorption determines the total acidity of the sample, that is Brønsted and Lewis acid sites, whereas the back-titration determines Brønsted sites only, and in fact, the acidity form back-titrations is always lower than that obtained from chemisorption.

Considering the importance that acidity has for the isomerization of sugars, diffuse reflectance infrared Fourier transform (DRIFT) spectroscopy, using pyridine as adsorbate, was carried out (Fig. 6), with the aim to distinguish between strong and weak Brønsted sites, as well as strong and weak Lewis sites [46].

Bands at *ca.* 1,542 cm^{-1} and 1,450 cm^{-1} are characteristic of Brønsted and Lewis acid sites respectively [44], involving the formation
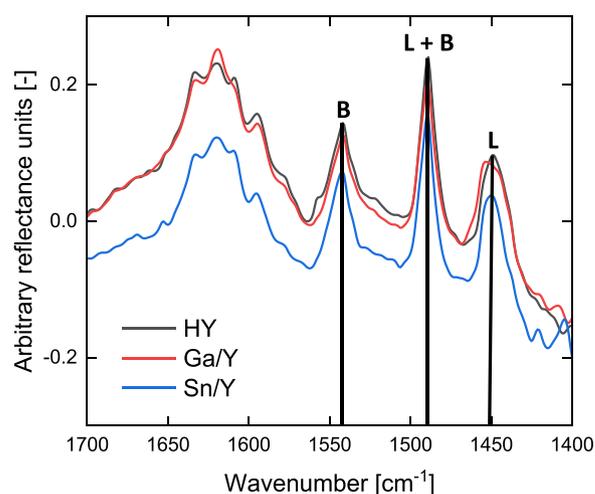
Fig. 6. DRIFT spectra of HY (black line), Sn/Y (blue line) and Ga/Y (red line) pre-treated with Ar and then adsorbed with pyridine at 150 °C. Vertical lines represent the band position for Brønsted (B), Lewis (L) and combined Brønsted and Lewis (B + L) acid centres.

of pyridinium ion and weak adsorption interactions. In the region at 1, 490 cm^{-1} it is possible instead to detect a combination of weaker Brønsted sites and stronger Lewis centres. However, as these are detected for all of our materials, it is reasonable to conclude that these are comprised of Al centres in all cases. From the peak intensities, an estimate of the Lewis to Brønsted (L/B) ratio is 0.95, 0.89, and 1.2 for HY, Sn/Y and Ga/Y respectively, which is consistent with the data from total Brønsted acidity and chemisorption (Table 4). That is a slight increase in Lewis acidity for the Ga/Y doped material.

These data were complemented by BET surface area and micropore volume of our materials (Table 4) which were carried out to identify if substantial changes in the density of the acid sites were present, but again these differences appear to be negligible. Furthermore, a small decrease in both surface area and micropore volume was observed upon doping, which is consistent with the preparation method used [45].

3.5.2. X-ray photoelectron spectroscopy and inductively coupled plasma analysis

In order to complement the acidity data reported above, X-ray photoelectron spectroscopy [47], was carried out to determine the chemical state and the amount of Sn and Ga centres in our materials. The chemical status of Sn is consistent with that of SnO_2 with binding energies for Sn $3d_{5/2}$ and Sn $3d_{3/2}$ of 495.4 eV and 486.7 eV respectively [48] (Fig. S12), whereas the XPS the signal of Ga is compatible with that of Ga_2O_3 with a binding energy for Ga $2p_{3/2} = 1{,}117.8$ eV or Ga in a high oxidation state [49] (Fig. S13). These chemical states for Sn and Ga are consistent with our preparation method (wetness impregnation and calcination in air) [45]. Although the isolated, or surface coordinatively unsaturated species, Sn^{4+} and Ga^{3+} are Lewis acid centres, SnO_2 and Ga_2O_3 are *per se* basic, which could explain the small apparent decrease in acidity observed from our acidity measurements. Quantification of the surface composition (Table 5), on the other hand, showed the materials to be rather different.

Whereas Sn was detected in a quite appreciable amount, 1.8 at %, the surface amount of Ga was far less, 0.1 at %, close to the detection limit (Figs. S12 and S13). If these amounts were to be contrasted with their expected bulk composition of 1 wt % for each of these two metals, a 1 wt % would correspond to *ca.* 0.5 mol % for Sn and 0.9 mol % for Ga for the entire bulk material (to compensate for this difference all our tests were at a constant molar metal to substrate ratio). In other words, if Sn and Ga were to be uniformly distributed within and on the surface of the zeolite, we would expect to detect more at % or mol % for Ga rather than Sn. As XPS is a surface method with an average penetration depth from 5 to 10 nm [50] the very weak signal detected for Ga would suggest that Ga is mainly *inside* the pores of the zeolites, whereas Sn is mainly distributed on the *surface* of the zeolite crystals.

3.5.3. High-angle annular dark-field imaging – Scanning transmission electron microscopy

In order to gain direct evidence from the conclusions inferred from XPS, that is Sn (in the form of SnO_2 clusters) is mostly on the surface of the zeolite crystals and Ga (in the form of Ga_2O_3 clusters) is mostly present inside the pores of the zeolite, the samples were analysed *via* high-angle annular dark-field imaging – scanning transmission electron microscopy (HAADF-STEM) [51]. It is possible to directly observe that

Sn/Y does indeed have defined SnO_2 clusters on the outside of the zeolite crystals (Fig. 7A) with an average particle size of 4.2 nm (Fig. 7B).

In contrast, Ga/Y did not show any obvious presence of Ga_2O_3 clusters (Fig. 8A) or only occasionally (Fig. 8B) leading us to conclude that Ga has to be indeed either highly dispersed or to be present inside the pores of the zeolite.

It is rather surprising to obtain a highly dispersed metal by using a straightforward impregnation protocol, and this could have implications beyond our study. This phenomenon has been rarely observed so far, like in the preparation of Fe doped mesoporous silica SBA-15 [52] or zeolite HZSM-5 [53], but only by using vacuum synthesis methods and with alkali metals as promoters. This is unlike the protocol used in this study, which is carried out at atmospheric pressure and without the addition of any alkali metals. Yet still, such a profound difference does not seem a major driving factor for this reaction. As such we conclude that the majority of the activity originates as a consequence of the acidity of the zeolite framework. Nevertheless, it is important to understand the effect that added dopant metals may have. For instance, speculations on the activity of metals like Sn and Ga based on their Lewis acidity should be carefully considered when moving, for example, from a homogenous system [11–13] to a heterogeneous one, as such retention of the activity may not persist. Though this can still have effects on selectivity.

3.5.4. Powder X-ray diffraction

Powder XRD patterns were collected for zeolite HY, Sn/Y and Ga/Y (Fig. 9). In order to assess if any ion exchange or distortion of the zeolite could have occurred as a consequence of the preparation method used. A Rietveld refinement [54] was carried out (Table S3). The XRD patterns look virtually identical, and no significant contraction of the unit cell volume of Sn/Y and Ga/Y was detected with respect to variations of the unit cell volume of the parent zeolite HY (calculated value 14377 Å^3). These data would rule out - at least within the acquired PXRD resolution - any incorporation of Sn or Ga into the zeolite framework in place of Al centres.

It may also be worth noting that although Sn and Ga were established to be present as SnO_2 and Ga_2O_3 (see Sections 3.5.2 and 3.5.3) no characteristic reflections for SnO_2 or Ga_2O_3 were detected. These were expected to be at 26.6°, 37.8° and 51.8° 2θ, for the reflections (110), (200) and (211) respectively for SnO_2 [50], and at 31.2°, 35.9° and 38.1° 2θ, for the reflections (222), (400) and (411) respectively for β-Ga_2O_3 [55]. This, however, is consistent with HAADF-STEM data and a particle size smaller than 4–5 nm, or highly dispersed metal species [56]. That is, crystals that are sufficiently small will lead to a very broad and therefore undetectable signal.

3.5.5. Extended X-ray absorption fine structure and structure considerations

To further corroborate our results and data interpretation from HAADF-STEM, and XRD concerning the structural properties of Sn/Y and Ga/Y, these catalysts were characterised by means of extended X-ray absorption fine structure (EXAFS) methods [57,58].

Firstly our EXAFS measurements showed the signal for Ga/Y was much higher than the signal for Sn/Y thus matching ICP-MS data showing a higher mol % of Ga with respect to Sn. Therefore, differences in the fitting of the species must be due to a different metal distribution of these two species within the materials studied.

Sn/Y was fitted against a SnO_2 standard [59], and the results of EXAFS interpolation are consistent with the crystallographic structure of SnO_2 (Fig. 10 and Table S4).

The only notable difference detected in our materials, with respect to a standard bulk SnO_2, is the higher Debye-Waller factor on the outer Sn shells (0.0089 Å^2) (Table S5). This suggests SnO_2 is slightly more disordered/amorphous with respect to a bulk oxide. As the bulk oxide is a well-ordered material, we would expect a value of 0.003–0.005 Å^2 for the photoelectron mean Sn-Sn path in the second shell.

The results for Ga/Y, analogous to HAADF-STEM data, are rather

Table 5

Atomic surface composition in at % for zeolites HY, Sn/Y and Ga/Y. The presence of carbon is adventitious, and all the other elements are consistent with the precursors used and the elemental composition for the framework of the zeolite.

Catalyst	At (%)							
	C	O	Sn	Si	Al	Ga	N	Cl
HY	11.0	56.8	0.0	30.8	1.3	0.0	0.1	0.0
Sn/Y	9.5	57.3	1.8	30.5	1.0	0.0	0.0	0.0
Ga/Y	10.0	59.6	0.0	29.0	1.0	0.1	0.2	0.0
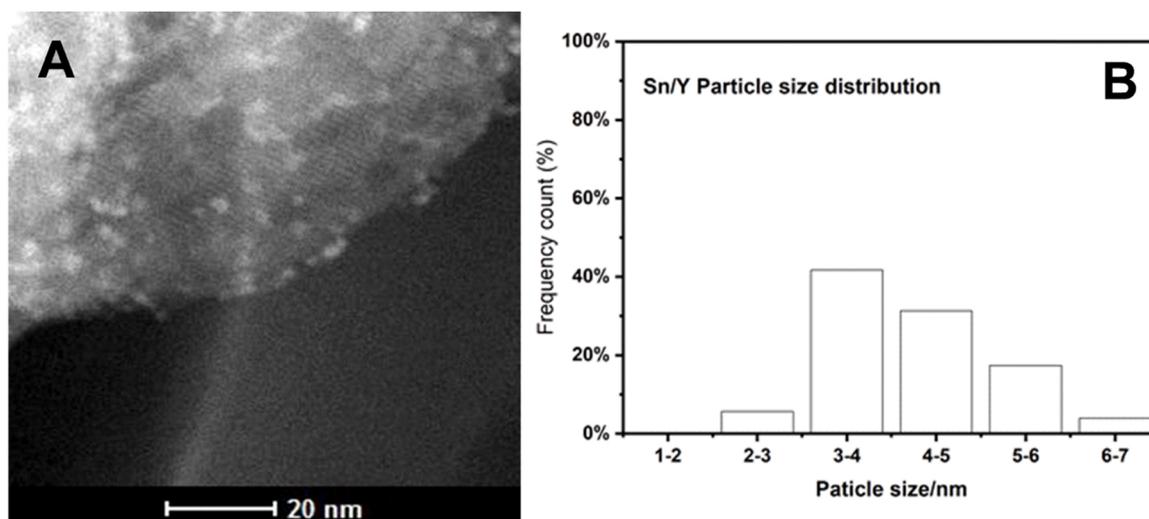
Fig. 7. . (A), HAADF-STEM image of a Sn/Y catalyst prepared *via* wetness impregnation with a Sn metal loading of 1 wt %. The fringe like structure on the support are the zeolite channels, and the particles at its edges, *i.e.* externally to the zeolite crystal are deposited nanoparticles consistent with SnO_2. (B), SnO_2 particle size distribution with an average particle size $d = 4.2$ nm.
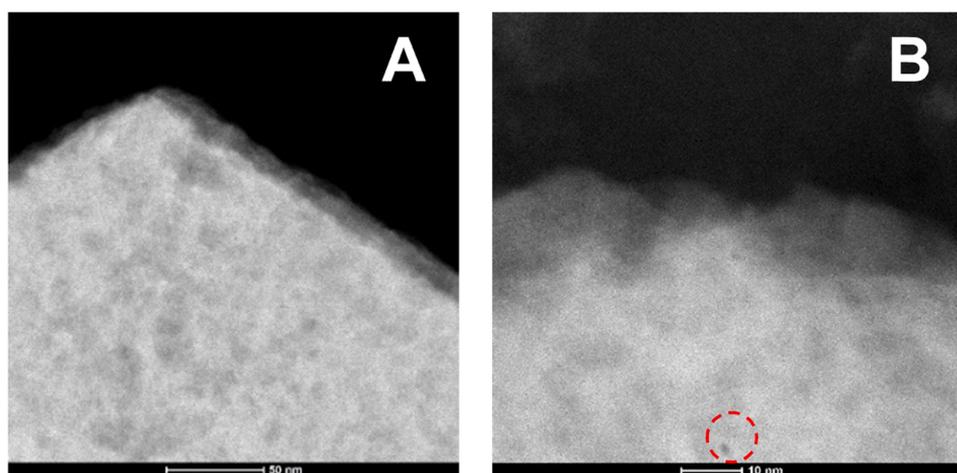
Fig. 8. HAADF-STEM image of a Ga/Y material prepared *via* wetness impregnation with a Ga metal loading of 1 wt %. (A) No presence of metal or metal nano-particles is observed outside the zeolite crystals, or (B) only occasionally (dark spot within the dashed red circle).

different. The EXAFS results were fitted by either assuming the presence of β-Ga_2O_3 clusters, or the incorporation of Ga into the zeolite framework. Moving to the Ga edge, and observing the data, it is clear to see the lack of a second shell in the EXAFS Fourier transform signal, which could be consistent with β-Ga_2O_3. In contrast, the first shell is consistent with the presence of 4 to 6 oxygen atoms, as for a Ga species incorporated within the zeolite framework [60]. A satisfactory fit is not possible with a scattering path involving Ga-Ga atoms from β-Ga_2O_3 crystal structure [61] (Fig. 11).

However, the fit improves dramatically when trying to replace Ga in the zeolite structure (Fig. 11, Table S5). The distances seem to reflect the higher atomic weight of Ga with respect to Si/Al, with a first shell distance almost identical to the Ga-O bond length in gallium oxide. The second shell intensity and phase are better reproduced, and they are shifted by the same amount (+0.2 Å). Also, in this case, the Debye-Waller factor is relatively high (0.02 $Å^2$), which suggests a strain/disorder in the structure.

4. Conclusions

In this work, we have clearly identified that the isomerization of

glucose to fructose is a complex process with multiple species interconverting each other, and involving the formation of a methyl fructoside intermediate and mannose when the reaction is carried out in methanol.

All the catalysts studied HY, Sn/Y and Ga/Y showed a similar conversion of glucose to fructose, methyl fructoside, and mannose with respect to the use of different reaction temperatures from 80 to 120 °C by using methanol, and methanol followed by the addition of water as the reaction solvent. Although the use of a higher temperature enhanced the glucose conversion above 90 % and fructose selectivity up to 50 %, the measured carbon mass balance implied that more by-products, likely humins, were formed. An optimal reaction temperature of 100 °C was identified as a result of these factors.

The use of methanol as a solvent, led to the production of large amounts of methyl fructoside intermediate as a reaction product produced *via* a reaction pathway promoted by Brønsted acid sites. When catalytic tests were performed using fructose and mannose as substrates and methanol as the reaction solvent, all zeolites led to a reaction mixture comprised of glucose, methyl fructoside, fructose and mannose. We could also demonstrate that glucose, fructose and mannose are in equilibrium with fructose *via* a hydride shift mediated by Lewis acid sites
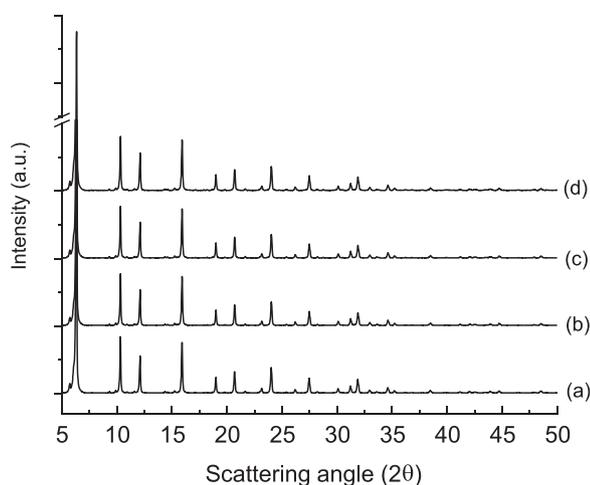
Fig. 9. X-ray powder diffraction patterns for zeolites: (a) HY as delivered, (b) HY treated as for metal deposition but without any metal dopant, (c) Sn/Y and (d) Ga/Y. No metal or metal oxide cluster from Sn or Ga is detected, and all zeolites present a virtually identical pattern.
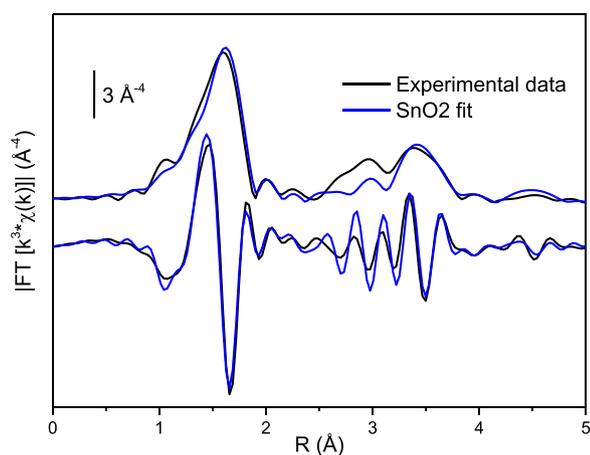
Fig. 10. EXAFS Fourier transform of a Sn/Y catalyst (black line). Spectra simulated using a model for SnO_2 clusters not part of the zeolite framework is represented by the blue line. An excellent fit consistent with slightly amorphous SnO_2 was obtained.
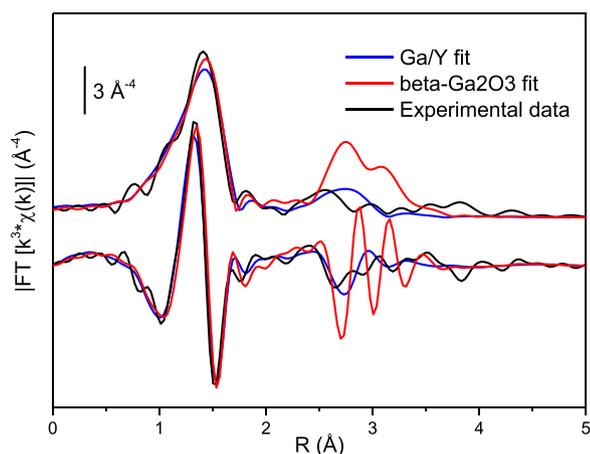
Fig. 11. EXAFS Fourier transform of a Ga/Y catalyst. Spectra simulated using a model considering: (red line) Ga_2O_3 clusters not part of the zeolite framework, and (blue line) Ga species as part of the zeolite framework. In the latter case an enhanced fit of the experimental data is obtained.

on the catalyst. Therefore, the conversion of glucose in methanol is a consequence of three reaction pathways: (i) a Lewis pathway capable of converting glucose to fructose, and then mannose, (ii) the reverse reaction, and (iii) a Brønsted catalysed water hydrolysis for the conversion of fructose to methyl fructoside.

If instead, the catalytic tests were carried out in the presence of water after methanol, this solvent could promote the hydrolysis of methyl fructoside to fructose whilst, at the same time, quenching the catalytic activity of all of the zeolite-based catalysts for the isomerization reaction of glucose to fructose. This is probably due to strong adsorption of water within the pores of the zeolites, or by a site-blocking of the Lewis acid sites responsible for the isomerization reaction. If, however, water was added after a reaction step in methanol, this solvent promoted the conversion of methyl fructoside to fructose in all cases, thus leading us to conclude that a Brønsted acid pathway is dominant for this reaction. This is likely to be the reason for the similar catalytic activity determined across the range of studied catalysts for this reaction.

Ga/Y and Sn/Y were found to differ significantly in structure with Sn/Y comprising SnO_2 clusters outside the zeolite crystals and Ga/Y presenting highly dispersed Ga species within the pores instead. Consequently, the Brønsted acid catalysed step discussed previously, may not necessarily occur or be constrained by the pores of the zeolite, and this will form the basis of additional investigations in order to ascertain the role of the pore size for this reaction when water is not used as a primary solvent.

CRediT authorship contribution statement

M.M.K.: Investigation, Writing – original draft, Formal analysis, Methodology, Writing – review and editing; **D.S.:** Methodology, Investigation; **J.R.:** Methodology, Investigation; **N.S.:** Resources, Methodology, Investigation; **P.J.C.:** Resources, Methodology, Investigation, Funding acquisition; **D.G.:** Resources, Methodology, Investigation, Writing – original draft; **G.C.:** Resources, Methodology, Investigation, Funding acquisition; **L.F.:** Methodology, Investigation, Writing – review and editing; **C.D'A.:** Methodology, Investigation Writing – review and editing; **X.L.:** Resources, Methodology, Investigation, Writing – review and editing, Funding acquisition; **L.C.:** Resources, Investigation, Funding acquisition; **V.D.:** Resources, Methodology, Investigation, Writing – review and editing; **M.C.:** Conceptualization, Methodology, Formal analysis, Visualization, Supervision, Funding acquisition, Writing – original draft, review and editing.

Declaration of Competing Interest

The authors declare that they have no known competing financial interests or personal relationships that could have appeared to influence the work reported in this paper.

Data Availability

All data supporting this study are provided in full in the 'Results' section of this paper and as Supplementary information accompanying this paper.

Acknowledgments

Supplementary material

HPLC-MS data, kinetic profiles, HPLC chromatograms, Rietveld refinement data, XPS spectra and EXFAS fitting results.

Appendix A. Supporting information

Supplementary data associated with this article can be found in the online version at doi:10.1016/j.apcata.2022.118689.

References

[1] I. Delidovich, R. Palkovits, ChemSusChem 9 (2016) 547–561.
[2] P. Gallezot, Chem. Soc. Rev. 41 (2012) 1538–1558.
[3] S. Dutta, ChemSusChem 5 (2012) 2125–2127.
[4] V. Choudhary, A.B. Pinar, R.F. Lobo, D.G. Vlachos, S.I. Sandler, ChemSusChem 6 (2013) 2369–2376.
[5] B. Kamm, Angew. Chem. Int. Ed. 46 (2007) 5056–5058.
[6] Palsdottir, D. Silverman, R.F. Lobo, L.A. Curtiss, M.E. Davis, Proc. Nat. Acad. Sci. USA 109 (2012) 9727–9732.
[7] N. Rai, S. Caratzoulas, D.G. Vlachos, ACS Catal 3 (2013) 2294–2298.
[8] M. Moliner, Y. Román-Leshkov, M.E. Davis, Proc. Nat. Acad. Sci. USA 107 (2010) 6164–6168.
[9] R. Bermejo-Deval, M. Orazov, R. Gounder, S.J. Hwang, M.E. Davis, ACS Catal. 4 (2014) 2288–2297.
[10] R. Oozeerally, J. Pillier, E. Kilic, P.B.J. Thompson, M. Walker, B.E. Griffith, J. V. Hanna, V. Degirmenci, Appl. Catal. A: Gen. 605 (2020), 117798.
[11] H. Nguyen, V. Nikolakis, D.G. Vlachos, ACS Catal. 6 (2016) 1497–1504.
[12] Y. Román-Leshkov, M. Moliner, J.A. Labinger, M.E. Davis, Angew. Chem. Int. Ed. 122 (2010) 9138–9141.
[13] G. Li, E.A. Pidko, E.J.M. Hensen, Catal. Sci. Technol. 4 (2014) 2241–2250.
[14] R. Fricke, H. Kosslick, G. Lischke, M. Richter, Chem. Rev. 100 (2000) 2303–2405.
[15] J.A. Lopez-Sanchez, M. Conte, P. Landon, W. Zhou, J.K. Bartley, S.H. Taylor, A. F. Carley, C.J. Kiely, K. Khalid, G.J. Hutchings, Catal. Lett. 142 (2012) 1049–1056.
[16] S. Saravanamurugan, M. Paniagua, J.A. Melero, A. Riisager, J. Am. Chem. Soc. 135 (2013) 5246–5249.
[17] M. Conte, J.A. Lopez-Sanchez, Q. He, D.J. Morgan, Y. Ryabenkova, J.K. Bartley, A. F. Carley, S.H. Taylor, C.J. Kiely, K. Khalid, G.J. Hutchings, Catal. Sci. Technol. 2 (2012) 105–112.
[18] N.C. Megoulas, M.A. Koupparis, Crit. Rev. Anal. Chem. 35 (2005) 301–316.
[19] S. Tantisriyanurak, H.N. Duguid, L. Peattie, R. Dawson, ACS Appl. Polym. Mater. 2 (2020) 3908–3915.
[20] C. Tyl, G.D. Sadler, pH and Titratable Acidity, in: S.S. Nielsen, S.S. (Eds.), Food Analysis. Food Science Text Series, Springer, Cham, 2017, pp. 389–406.
[21] M. Conte, B. Xu, T.E. Davies, J.K. Bartley, A.F. Carley, S.H. Taylor, K. Khalid, G. J. Hutchings, Microporous Mesoporous Mater. 164 (2012) 207–213.
[22] P.R. Davies, N.G. Newton, Surf. Sci. 546 (2003) 149–158.
[23] Y.S. Ding, X.F. Shen, S. Sithambaram, S. Gomez, R. Kumar, V.M.B. Crisostomo, S. L. Suib, M. Aindow, Chem. Mater. 17 (2005) 5382–5389.
[24] F. Sánchez-Bajo, F.L. Cumbrera, J. Appl. Crystallogr. 32 (1999) 730–735.
[25] R.J. Hill, L.M.D. Cranswick, J. Appl. Crystallogr. 27 (1994) 802–844.
[26] Crystallographic information files made by reference to ⟨http://www.izastructure. org/databases/⟩.
[27] D. Briggs, G. Beamson, Anal. Chem. 64 (1992) 1729–1736.
[28] A.J. Dent, G. Cibin, S. Ramos, A.D. Smith, S.M. Scott, L. Varandas, M.R. Pearson, N. A. Krumpa, C.P. Jones, P.E. Robbins, J. Phys. Conf. Ser. 190 (2009), 012039.
[29] B. Ravel, M. Newville, J. Synchrotron Radiat. 12 (2005) 537–541.
[30] J.J. Rehr, R.C. Albers, Rev. Mod. Phys. 72 (2000) 621–654.
[31] N. Rajabbeigi, A.I. Torres, C.M. Lew, B. Elyassi, L. Ren, Z. Wang, H. Je Cho, W. Fan, P. Daoutidis, M. Tsapatsis, Chem. Eng. Sci. 116 (2014) 235–242.
[32] R. Gounder, M.E. Davis, AIChE J. 59 (2013) 3349–3358.
[33] R. Bermejo-Deval, R. Gounder, M.E. Davis, ACS Catal. 2 (2012) 2705–2713.
[34] M. Demerdash, R.M. Attia, Zentralbl. Mikrobiol. 147 (1992) 297–303.
[35] J. Cui, J. Tan, T. Deng, X. Cui, Y. Zhu, Y. Li, Green Chem. 18 (2016) 1619–1624.
[36] F.A.J. Meskens, Synthesis 1981 (1981) 501–522.
[37] D.M. Gao, T. Kobayashi, S. Adachi, Bioscience, Biosci. Biotechnol. Biochem. 79 (2015) 1005–1010.
[38] V.F. Taylor, R.E. March, H.P. Longerich, C.J. Stadey, Int. J. Mass Spectrom. 243 (2005) 71–84.
[39] M.L. Hayes, N.J. Pennings, A.S. Serianni, R. Barker, J. Am. Chem. Soc. 104 (1982) 6764–6769.
[40] S. Osanai, in: Glycoscience, Stütz A.E. (Ed.), Berlin, Heidelberg, 2001, pp. 43–76.
[41] S. Bhunia, B. Banerjee, A. Bhaumik, Chem. Commun. 51 (2015) 5020–5023.
[42] R.M.N. Kalla, M.-R. Kim, I. Kim, Ind. Eng. Chem. Res. 57 (2018) 11583–11591.
[43] R. Weingarten, G.A. Tompsett, W.C. Conner Jr., G.W. Huber, J. Catal. 279 (2011) 174–182.
[44] A. Platon, W.J. Thomson, Ind. Eng. Chem. Res. 42 (2003) 5988–5992.
[45] M. Conte, J.A. Lopez-Sanchez, Q. He, D.J. Morgan, Y. Ryabenkova, J.K. Bartley, A. F. Carley, S.H. Taylor, C.J. Kiely, K. Khalid, G.J. Hutchings, Catal. Sci. Technol. 2 (2012) 105–112.
[46] M. Valdés, F.J. Ulloa, V.A. Solar, M.S. Cepeda, F. Azzolina-Jury, F. Thibault-Starzyk, Microporous Mesoporous Mater. 294 (2020), 109912.
[47] C.A. Wilde, Y. Ryabenkova, I.M. Firth, L. Pratt, J. Railton, M. Bravo-Sanchez, N. Sano, P.J. Cumpson, P.D. Coates, X. Liu, M. Conte, Appl. Catal. A: Gen. 570 (2019) 271–282.
[48] H. Willemen, D.F. van de Vondel, G.P. van der Kelen, Inorg. Chim. Acta 34 (1979) 175–180.
[49] G. Schön, J. Electron Spectrosc. Relat. Phenom. 2 (1973) 75–86.
[50] M. Conte, C.J. Davies, D.J. Morgan, T.E. Davies, D.J. Elias, A.F. Carley, P. Johnston, G.J. Hutchings, J. Catal. 297 (2013) 128–136.
[51] J. Zhang, S. Nagamatsu, J. Du, C. Tong, H. Fang, D. Deng, X. Liu, K. Asakura, Y. Yuan, J. Catal. 367 (2018) 16–26.
[52] Y. Li, Y. Chen, L. Li, J. Gu, W. Zhao, L. Li, J. Shi, Appl. Catal. A: Gen. 366 (2009) 57–64.
[53] J. Ma, D. Weng, X. Wu, Z. Si, Z. Wu, Prog. Nat. Sci. Mater. 23 (2013) 493–500.
[54] L.B. McCusker, R.B. Von Dreele, D.E. Cox, D. Louër, P. Scardi, J. Appl. Crystallogr. 32 (1999) 36–50.
[55] R. Roy, V.G. Hill, E.F. Osborn, J. Am. Chem. Soc. 74 (1952) 719–722.
[56] J.O. Weston, H. Miyamura, T. Yasukawa, D. Sutarma, C.A. Baker, P.K. Singh, M. Bravo-Sanchez, N. Sano, P.J. Cumpson, Y. Ryabenkova, S. Kobayashi, M. Conte, Catal. Sci. Technol. 7 (2017) 3985–3998.
[57] N. Senamart, S. Buttha, W. Pantupho, I.Z. Koleva, S. Loiha, H.A. Aleksandrov, J. Wittayakun, G.N. Vayssilov, J. Porous Mater. 26 (2019) 1227–1240.
[58] C. Genovese, M.E. Schuster, E.K. Gibson, D. Gianolio, V. Posligua, R. Grau-Crespo, G. Cibin, P.P. Wells, D. Garai, V. Solokha, S. Krick Calderon, J.J. Velasco-Velez, C. Ampelli, S. Perathoner, G. Held, G. Centi, R. Arrigo, Nat. Commun. 9 (2018) 935.
[59] Y.-I. Kim, M.-J. Jung, K.-H. Kim, J. Korean Ceram. Soc. 6 (2000) 354–358.
[60] S.A. Axon, K. Huddersman, J. Klinowski, Chem. Phys. Lett. 172 (1990) 398–404.
[61] N.S. Smirnova, D.A. Shlyapin, O.O. Mironenko, E.A. Anoshkina, V.L. Temerev, N. B. Shitova, D.I. Kochubey, P.G. Tsyrul`Nikov, J. Mol. Catal. A Chem. 358 (2012) 152–158.